Sensorless Speed Control for Dual Stator Induction Motor Drive Using IFOC Strategy with Magnetic Saturation

Marwa Ben Slimene, Mohamed Arbi Khlifi, and Mouldi Ben Fredj

Department of Electrical Engineering
ENSIT, University of Tunis, Taha Hussein, BP 56, 1008 Tunis, Tunisia
Mohamedarbi.khlifi@issatm.rnu.tn, benslimene.marwa@gmail.com

Abstract ─ A method of a sensorless indirect rotor-field-oriented control of a dual stator induction motor with magnetic saturation is proposed in this paper. Magnetic characteristics of the dual stator induction motor indicate a nonlinear behavior. The computational electromagnetic d-q model when the dual stator are fed by an independently current-controlled pulse width modulation (PWM) two identical three-phase voltage source inverters. By controlling the machine's phase currents, harmonic elimination and torque ripple reduction techniques could be observed. The unbalanced current sharing between the dual stator winding sets is eliminated. High accuracy and performance is obviously demonstrated by comparing experimental and simulation results both in electromagnetic and dynamic features.

Index Terms ─ Dual Stator Induction Machine (DSIM), Field Oriented Control (F.O.C), magnetic saturation, magnetizing inductance.

I. INTRODUCTION

Actually, electromagnetic simulators are essential tools in the analysis and the design of large and complex systems especially the industrial electrical drives. Cost, reliability, robustness and maintenance free operation are among the reasons these machines are replacing DC drive systems. The last two decades have witnessed dramatic improvements in both algorithms for computational electromagnetics and computing hardware [1-3]. However, when an ac machine is supplied from an inverter, the need for a predefined number of phases on stator, such as three, disappears and other phase numbers can be chosen. The early interest in multiphase machines was caused by the possibility of reducing the torque pulsations, minimizing the magnetic flux harmonic, improved reliability and reduction on the power ratings for the static converter [4-5]. In particular, with loss of one or more of stator winding excitation sets, a multi-phase induction machine can continue to be operated with an asymmetrical winding structure and unbalanced excitation [6-7]. By dividing the required power between multiple phases, higher power levels can be obtained and the limits of number of machine phases have been removed when employing voltage source inverter [8-9]. The use of multi-phase machines permits to take advantage of additional degrees of freedom but is likely limited to specialized applications such as electric/ hybrid vehicles, aerospace applications, ship propulsion, and high power application [10-11]. Such a machine, addition to the power segmentation and redundancy it carries, has the advantage of reducing the torque pulsations, rotor losses and the reduction of harmonic current [12-13]. However, the introduction of magnetic nonlinearities in the electrical equations operating has always been a topical issue for polyphase machines. Indeed, taking into account the saturation is not simply dictated by the desire to improve the results, but it can sometimes be a necessity.

One of the most important parts in the modeling of DSIM with closed magnetic circuit is magnetic characteristics of motor. They are directly in correlation with electrical and mechanical subsystems. Moreover, nonlinear behavior of magnetic characteristics makes the nonlinear model and more complex [14-15].

In order to achieve a mathematical model the leakage mutual inductance effect is investigated. In this paper, a nonlinear model including experimental characteristic is proposed to attain transient magnetic characteristics. The specific issue of current control is the problem of unbalanced current sharing between the two three-phase winding sets, due to the small system asymmetries that cannot be eliminated, [16]. In this paper, a d-q model of the dual stator induction machine (DSIM) is developed in a general reference frame and the effect of mutual leakage inductance and magnetic saturation are included. Subsequently, an indirect rotor-field-oriented control for the DSIM is presented and detailed with 0 and 30 electrical degrees shift between the two three phase winding sets. Simulation results are provided to demonstrate the validity of proposed control.

II. COMPUTATIONAL ELECTROMAGNETIC D-Q MODEL OF DSIM

A. Transient model

A common type of multiphase machine is the dual stator induction machine (DSIM), where two sets of three-phase windings, spatially phase shifted by 30 electrical degrees, share a common stator magnetic core as shown in
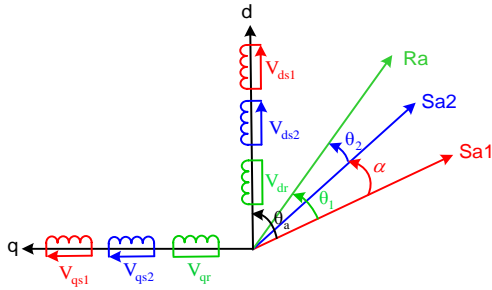
Fig. 1.

Fig. 1. DSIM windings.

The voltage equations of the dual stator induction machine using decomposition vector space are as follow. For the stator circuit we can write:

$$\begin{cases} V_{ds1} = R_s.i_{ds1} + \dfrac{d\lambda_{ds1}}{dt} - w_a\lambda_{qs1} \\[2mm] V_{qs1} = R_s.i_{qs1} + \dfrac{d\lambda_{qs1}}{dt} + w_a\lambda_{ds1} \\[2mm] V_{ds2} = R_s.i_{ds2} + \dfrac{d\lambda_{ds2}}{dt} - w_a\lambda_{qs2} \\[2mm] V_{qs2} = R_s.i_{qs2} + \dfrac{d\lambda_{qs2}}{dt} + w_a\lambda_{ds2} \end{cases} . \qquad (1)$$

And for the rotor circuit we have:

$$\begin{cases} 0 = R_r.i_{dr} + \dfrac{d\lambda_{dr}}{dt} - (w_a - w)\lambda_{qr} \\[2mm] 0 = R_r.i_{qr} + \dfrac{d\lambda_{qr}}{dt} + (w_a - w)\lambda_{dr} \end{cases} , \qquad (2)$$

where w_a is the speed of the reference frame.

Such as l_{sm} is the common mutual leakage inductance between the two sets of stators windings, L_m is the mutual inductance between stator and rotor, l_s, l_r are the stator and rotor leakage inductance respectively, where

$$\begin{cases} L_s = l_s + l_{sm} + L_m \\ L_r = l_r + L_m \\ L_{ps} = l_{sm} + L_m \\ M = L_m \end{cases} . \qquad (3)$$

The writing matrix of flux is characterized by the following relationship:

$$\begin{bmatrix} \lambda_{ds1} \\ \lambda_{qs1} \\ \lambda_{ds2} \\ \lambda_{qs2} \\ \lambda_{dr} \\ \lambda_{qr} \end{bmatrix} = \begin{bmatrix} L_s & 0 & L_{ps} & 0 & M & 0 \\ 0 & L_s & 0 & L_{ps} & 0 & M \\ L_{ps} & 0 & L_s & 0 & M & 0 \\ 0 & L_{ps} & 0 & L_s & 0 & M \\ M & 0 & M & 0 & L_r & 0 \\ 0 & M & 0 & M & 0 & L_r \end{bmatrix} \begin{bmatrix} i_{ds1} \\ i_{qs1} \\ i_{ds2} \\ i_{qs2} \\ i_{dr} \\ i_{qr} \end{bmatrix} . \qquad (4)$$

B. Flux linkage determination

The magnetic characteristic data of the linear actuators is obtained from experimental measurements. In order to complete the actuator modeling, data should be employed properly. The method consists to use the data of flux M is to approximate $M\text{-}x\text{-}i_m$ characteristics employing polynomial functions. The main advantage of this method is significant decrease in the calculations complexity. Nevertheless, the relatively much increase of the error in the extrapolation is the fundamental disadvantage. The current increase results in decrease in the flux linkage increase rate, whereas in the polynomial approximation, the estimated value of the flux linkage out of the relevant range might get large values. Since for the large values of ac current, there is restriction in the characteristic measurement, this issue is regarded as a significant disadvantage. By contrast, the actuator can easily operate in high DC currents. On the other hand, in the short-term over currents and transient situations, the amount of winding current could be increased in comparison with the nominal current. However, a proper model must predict the behavior of the system with the minimum error in different situations.

The magnetization curve shown in Fig. 2 was approximated by a polynomial of order 7:

$$M = L_m = k_1 i_m^7 + k_2 i_m^6 + k_3 i_m^5 + k_4 i_m^4 + k_5 i_m^3 + k_6 i_m^2 + k_7 i_m + k_8;$$

$$k_1 = 0.19303; \quad k_2 = -1.4276;$$
$$k_3 = 4.3069; \quad k_4 = -6.8637;$$
$$k_5 = 6.4026; \quad k_6 = -3.8101;$$
$$k_7 = 1.2896; \quad k_8 = 0.51665;$$

Thus, the saturation effect is taken into account by the expression of the static and dynamic magnetizing inductances with respect to the magnetizing current. They are evaluated from the open circuit d-axis magnetizing curve $\lambda_m = f(i_m)$:

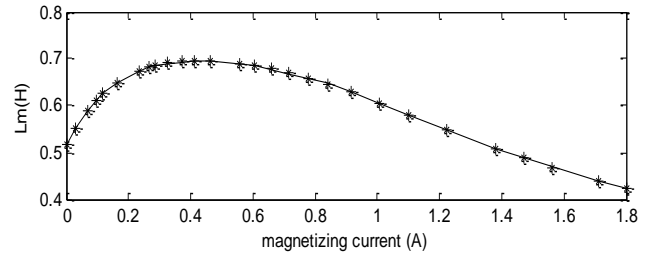$$L_m = \frac{\lambda_m}{i_m} \qquad L_{mdy} = \frac{d\lambda_m}{di_m}. \qquad (5)$$

Fig. 2. Approximation of magnetizing curve.

III. PROPOSED CONTROL STRATEGY

A. Derivation of indirect rotor-field oriented control of DSIM

We can determine the reference torque to impose on

the motor and the speed reference from the electromagnetic torque equation expressed in terms of Park's components, as shown in Fig. 3. If we impose the current we should preserve the torque proportional to the quadrature current. The resultant rotor flux λ_r, also known as the rotor-flux linkages phasor, is assumed to be on the direct axis, which corresponds with the reality, that the rotor flux linkages are a single variable. Hence, aligning the d axis with the rotor flux phasor yields such as:

$$\begin{cases} \lambda_{dr} = \lambda_r^* \\ \lambda_{qr} = 0 \end{cases}. \tag{6}$$

The rotor currents in terms of the stator currents are derived from (3) as:

$$\begin{cases} i_{dr} = \dfrac{\lambda_r^* - M(i_{ds1} + i_{ds2})}{L_r} \\ i_{qr} = \dfrac{-M}{L_r}(i_{qs1} + i_{qs2}) \end{cases}. \tag{7}$$

Substituting for direct and quadrature rotor currents from (9) into (2), the following are obtained:

$$\begin{cases} i_{ds1}^* + i_{ds2}^* = \dfrac{1}{M}\lambda_r^* + \dfrac{T_r}{M}\dfrac{d\lambda_r^*}{dt} \\ i_{qs1}^* + i_{qs2}^* = \dfrac{L_r}{n_p M}C_{em}^*\dfrac{1}{\lambda_r^*} \\ w_g^* = \dfrac{M}{T_r}\dfrac{1}{\lambda_r^*}(i_{qs1}^* + i_{qs2}^*) \end{cases}, \tag{8}$$

where

$$T_r = \dfrac{L_r}{R_r}, \tag{9}$$

T_r denotes the rotor time constant. Equation (9) resembles the field equation in a separately excited DC machine, whose time constant is usually on the order of seconds.

Similarly, the same substitution of the rotor currents from (8) into the electromagnetic torque and stator flux expressions such as:

$$C_{em}^* = n_p \dfrac{M}{L_r}\lambda_r^*(i_{qs1}^* + i_{qs2}^*), \tag{10}$$

$$\begin{cases} \lambda_{ds1} = \sigma_1 L_s i_{ds1} + \sigma_2 L_{ps} i_{ds2} + \dfrac{M}{L_r}\lambda_{dr} \\ \lambda_{qs1} = \sigma_1 L_s i_{qs1} + \sigma_2 L_{ps} i_{qs2} \\ \lambda_{ds2} = \sigma_2 L_{ps} i_{ds1} + \sigma_1 L_s i_{ds2} + \dfrac{M}{L_r}\lambda_{dr} \\ \lambda_{qs2} = \sigma_2 L_{ps} i_{qs1} + \sigma_1 L_s i_{qs2} \end{cases}, \tag{11}$$

where

$$\sigma_1 = 1 - \dfrac{M^2}{L_s L_r}; \quad \sigma_2 = 1 - \dfrac{M^2}{L_{ps} L_r}.$$

By introducing stator flux expressions into voltage expressions of the DSIM (1), the following are obtained:

$$\begin{cases} V_{ds1}^* = R_s i_{ds1} + (\sigma_1 L_s - \sigma_2 L_{ps})\dfrac{di_{ds1}}{dt} - w_s^*\left((\sigma_1 L_s - \sigma_2 L_{ps})i_{qs1} + \dfrac{\sigma_2 L_{ps} T_r}{M}w_g^*\lambda_r^*\right) \\ V_{qs1}^* = R_s i_{qs1} + (\sigma_1 L_s - \sigma_2 L_{ps})\dfrac{di_{qs1}}{dt} + w_s^*\left((\sigma_1 L_s - \sigma_2 L_{ps})i_{ds1} + \left(\dfrac{M}{L_r} + \dfrac{\sigma_2 L_{ps}}{M}\right)\lambda_r^*\right) \\ V_{ds2}^* = R_s i_{ds2} + (\sigma_1 L_s - \sigma_2 L_{ps})\dfrac{di_{ds2}}{dt} - w_s^*\left((\sigma_1 L_s - \sigma_2 L_{ps})i_{qs2} + \dfrac{\sigma_2 L_{ps} T_r}{M}w_g^*\lambda_r^*\right) \\ V_{qs2}^* = R_s i_{qs2} + (\sigma_1 L_s - \sigma_2 L_{ps})\dfrac{di_{qs2}}{dt} + w_s^*\left((\sigma_1 L_s - \sigma_2 L_{ps})i_{ds2} + \left(\dfrac{M}{L_r} + \dfrac{\sigma_2 L_{ps}}{M}\right)\lambda_r^*\right) \end{cases}.$$

Considering that the first parts of voltages expressions are the linear parts and adding PI currents regulations to achieve perfect decoupling:

$$\begin{cases} V_{ds1l} = R_s i_{ds1} + L\dfrac{di_{ds1}}{dt} \\ V_{qs1l} = R_s i_{qs1} + L\dfrac{di_{qs1}}{dt} \\ V_{ds2l} = R_s i_{ds2} + L\dfrac{di_{ds2}}{dt} \\ V_{qs2l} = R_s i_{qs2} + L\dfrac{di_{qs2}}{dt} \end{cases}, \tag{12}$$

where

$$L = \sigma_1 L_s - \sigma_2 L_{ps}. \tag{13}$$

The first reason for introducing the current control is the elimination of stator dynamics. Adding compensation terms to make d-q axes completely independent. So we pose the following system which compensates the errors producing during the operations of decoupling:

$$\begin{cases} V_{ds1}^* = V_{ds1l} - V_{ds1c} \\ V_{qs1}^* = V_{qs1l} + V_{qs1c} \\ V_{ds2}^* = V_{ds2l} - V_{ds2c} \\ V_{qs2}^* = V_{qs2l} - V_{qs2c} \end{cases}, \tag{14}$$

$$\begin{cases} V_{ds1c} = w_s^*\left(L i_{qs1} + \dfrac{\sigma_2 L_{ps} T_r}{M}w_g^*\lambda_r^*\right) \\ V_{qs1c} = w_s^*\left(L i_{ds1} + \left(\dfrac{M}{L_r} + \dfrac{\sigma_2 L_{ps}}{M}\right)\lambda_r^*\right) \\ V_{ds2c} = w_s^*\left(L i_{qs2} + \dfrac{\sigma_2 L_{ps} T_r}{M}w_g^*\lambda_r^*\right) \\ V_{qs2c} = w_s^*\left(L i_{ds2} + \left(\dfrac{M}{L_r} + \dfrac{\sigma_2 L_{ps}}{M}\right)\lambda_r^*\right) \end{cases}. \tag{15}$$
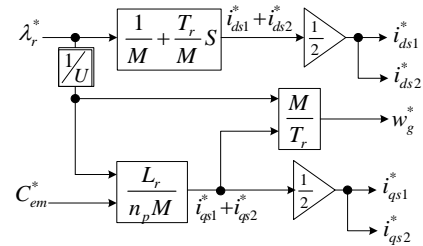
Fig. 3. Bloc of indirect rotor field-oriented.

B. Synthesis of regulators

The control of the stator current is ensured by a PI regulator and the reference rotor flux is given by a weakening-bloc which allows the working of the machine beyond the nominal speed. The PI controller parameters K_p and K_i are determined by pole placement method developed for the linear systems. The closed loop is given in Fig. 4. The closed loop transfer function is given by:

$$\frac{i_{ds1}}{i_{ds1}^*} = \frac{K_i S + K_p}{S^2 + \left(\dfrac{R_s + K_{pi}}{L}\right) S + \dfrac{K_{ii}}{L}}. \tag{16}$$

To get a well damped behavior, we use the poles placement approach.

Let $S = \rho_i \pm j\rho_i$, by identification, we obtain the parameters values of PI corrector based on p:

$$\begin{cases} K_p = 2\rho_i L - R_s \\ K_i = 2\rho_i^2 L \end{cases}. \tag{17}$$

Same calculation procedure for the other currents i_{qs1}, i_{ds2} and i_{qs2}. The speed control is simplified by the following diagram closed loop speed control is given in Fig. 5.

By applying the same procedure for calculating PI controller parameters stated above, we will have the following parameters:

$$\begin{cases} K_{pw} = 2\rho_w J - K_f \\ K_{iw} = 2\rho_w^2 J \end{cases}. \tag{18}$$
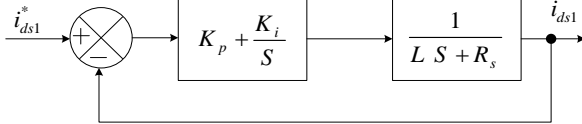
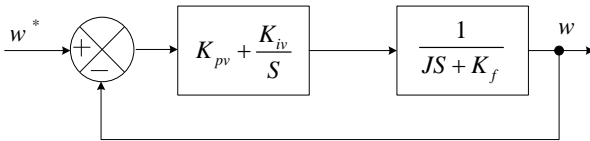

Fig. 4. Closed loop stator current.

Fig. 5. Closed loop speed control.

C. Implementation of indirect vector control scheme for DSIM (IFOC)

Using the proposed control strategy, the IFOC of a double stator induction motor drive supplied by two CRPWM is shown in Fig. 6. This allows a simple extension of the IFOC principle in that the rotor flux linkage is maintained entirely in the d-axis, resulting in the q-axis component of rotor flux being maintained at zero. This

reduces the electromagnetic torque equation to the same form as that of a dc machine or a rotor flux oriented three-phase machine. Thus, the electromagnetic torque and the rotor flux can be controlled independently, by controlling the d and q components of stator current. For this purpose, a vector control receives the speed and rotor flux requests and generates the commanded values of torque and flux producing components of stator current i_{ds1}^*, i_{ds2}^* and i_{qs1}^*, i_{qs2}^* respectively, which is processed through a proportional integral (PI) controller. The outputs of the four currents regulators, after an inverse Park transformation, are the stator voltage reference components in stationary reference frame to be applied to the PWM technique. For this purpose, the two sets of double stator currents are independently controlled and kept balanced for all possible operational conditions.
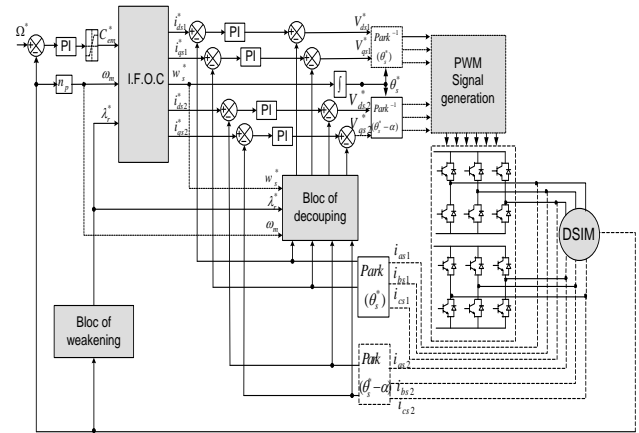

Fig. 6. Indirect rotor field-oriented control scheme for DSIM drive.

IV. ELECTROMAGNETIC SIMULATION AND EXPERIMENTAL RESULTS

A. Effect of flux linkage in DSIM

Though, the theory of main flux saturation is well recognized, a short application on DSIM is added to verify the validity impact of cross saturation in DSIM. Also, the objective of this application is to initially show comparison between models with cross magnetizing and without cross saturation on the machine operating. For that purpose this application treats the build-up of voltage and current during the dual stator induction motor (DSIM). The stator of each machine is rewound specifically for the task with two sets of three phase windings (two stars), Spatial shifting $\theta = 0^o$ between the two stars. The machine is star connected for all tests. The saturation curve was measured with the machine driven at synchronous speed. Figures 7, 8 and 9 simulates at no load the process of build-up of torque, current and air speed respectively, under rated speed.
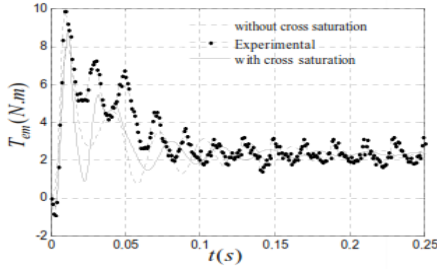
Fig. 7. Comparison between measured transient torque and simulated torque characteristics.
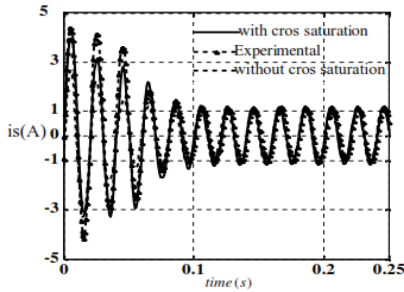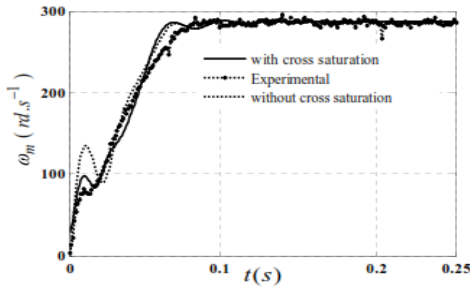

Fig. 8. Stator current of DSIM at load.

Fig. 9. Comparison between measured and simulated rotor transient rotor speed characteristics.

It is found that the time taken to reach the steady state for accurate model is about to the same for experimental results. Based on these results, we can conclude then, that the starting torque developed by the machine where we take into account main flux saturation is closer to the measurement result that the linear regime.

We also note that at start-up, the rotor speed of the DSIM, if taking into account the saturation with and without cross saturation is closer to the rotor speed measured than if ignored. We can confirm that the impact of the saturation model is clearer in transient regime and especially at start-up.

B. IRFOC control strategy of saturated DSIM

The IFOC control algorithm and precision of is verified using the simulation. It was proven that it is possible to achieve robust and reliable speed sensorless control, with satisfactory performance characteristics.

Furthermore, a novel modulation technique allowed for the improvement of control efficiency.

The proposed theoretical consideration of applying known sensorless control principles to a DSIM are verified using computational software. The simulation results show the successful implementation of sensorless speed estimation and decoupled vector control for DSIM. Separate stages, with different sampling times, for current and speed control are set in the simulation.

Speed estimation technique is verified using speed closed control loop for the DSIM with IFOC principles implemented. The flux was set to the nominal value, and the machine was first accelerated to the reference speed of 300 rad/s, while the load torque was kept at zero.

In Fig. 10, DSIM actual and estimated speed is presented, where the obvious transitions of torque and speed can be noted. In addition, the estimated and actual speed match almost perfectly providing the strong ground for practical speed sensorless drive implementation. High precision of speed estimation will ensure decoupled control for IFOC strategy, aligning the synchronous rotating reference frame to the desired position.

As shown in Fig. 10 (b), there seems to be no speed change when a step load change is effected as the large speed range selected for y-axes speed. When y-axis is zoomed, there is a speed variation of 0.7 rad/s, as observed in the extended view of speed.
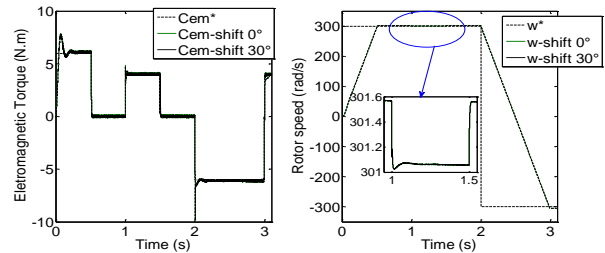

Fig. 10. (a) Electromagnetic torque and (b) rotor speed.

On the results shown in Fig. 11, one can see a high performance stator current response obtained despite the disturbance, and zoom to show the difference between the shift0 and shift30. From these waveforms, it is obvious that the ideal IRFOC is achieved in all working conditions.
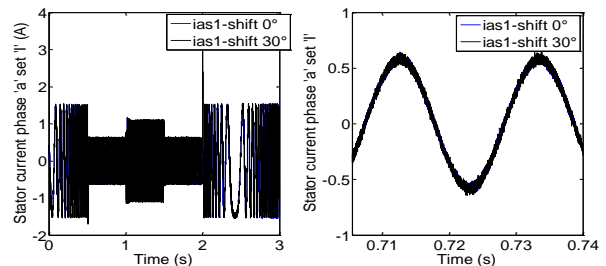

Fig. 11. Stator current per phase 'a' set 'I' for 0° and 30° shift.

The simulations were also carried out in order to verify the performance of the proposed indirect FOC scheme. The conventional method of field weakening (i.e., to vary the rotor flux reference in proportional to inverse of the rotor speed) was employed, and a step change of load torque 4 N.m at 1.0s was effected.

It is evident from the all pervious simulations results, that there is a very close correlation between the reference and simulated value of torque, current, speed and flux. It can also be clearly adjudged that there is no current unbalance between the two sets of stator windings. It is worth mentioning here that, in all the simulation work, the effect of mutual coupling l_{sm} has been included.

VI. CONCLUSION

In this paper, the vector control is introduced in order to control the dual stator induction motor with maximum power. It is based on a transient model with electromagnetic saturation. It allows precise adjustment of the electromagnetic torque of the machine and can ensure torque at zero speed. In this paper, we have presented the principle of the dual stator induction motor field oriented control, fed by a voltage inverter in the presence of a speed loop with a PI corrector. We can conclude that the field oriented control has a good dynamic and static electromagnetic torque, currents and flux results. We have proposed a simple approach for indirect rotor-field-oriented-control for DSIM drive fed by PWM two identical VSI and verified it by simulations when the acquired waveforms show good results. The effect of mutual leakage inductance between the two stator winding sets has been included in the model. For 30° shift, we concluded a reduction in torque ripples and the rotor heating is also reduced due to reduction in rotor currents. The comparison in experimental and simulation fields demonstrates a proper accuracy for the proposed dynamic modeling.

REFERENCES

[1] T. Yuvaraja and K. Ramya, "Vector control of PMSM take over by photovoltaic source," *ACES Express Journal*, vol. 1, no. 6, June 2016.

[2] M. R. Barzegaran, A. Sarikhani, and O. A. Mohammed, "An optimized equivalent source modeling for the evaluation of time harmonic radiated fields from electrical machines and drives," *Applied Computational Electromagnetics Society (ACES) Journal*, vol. 28, no. 4, pp. 273-283, Apr. 2013.

[3] B. S. Marwa, A. K. Mohamed, B. F. Mouldi, and R. Habib, "Analysis of saturated self-excited dual stator induction generator for wind energy generation," *Journal of Circuits, Systems, and Computers*, vol. 24, no. 9, pp. 196-203, 2015.

[4] B. S. Marwa, A. K. Mohamed, B. F. Mouldi, and R. Habib, "Modeling of dual stator induction generator with and without cross saturation," *Journal of Magnetics*, vol. 20, no. 3, pp. 165-171, 2015.

[5] E. Aycicek, N. Bekiroglu, I. Senol, and Y. Oner, "Rotor configuration for cogging torque minimization of the open slot structured axial flux permanent magnet synchronous motors," *ACES Journal*, vol. 30, no. 4, Apr. 2015.

[6] R. Sadouni and A. Meroufel, "Indirect rotor field-oriented control (IRFOC) of a dual star induction machine (DSIM) using a fuzzy controller," *Acta Polytechnica Hungarica.*, vol. 9, no. 4, pp. 177-192, 2012.

[7] A. S. Abdel-Khalik, M. I. Masoud, and B. W. Williams, "Vector controlled multiphase induction machine: Harmonic injection using optimized constant gains," *Electric Power Systems Research*, vol. 89, no. 15, pp. 116-128, 2012.

[8] B. S. Marwa, A. K. Mohamed, B. F. Mouldi, and R. Habib, "Effect of the stator mutual leakage reactance of dual stator induction generator," *International Journal of Electrical Energy*, vol. 2, no. 3, pp. 1810-1818, 2014.

[9] M. B. Slimene and M. A. Khlifi, "Performance limits of three-phase self-excited induction generator (SEIG) as a stand alone DER," *Journal of Electrical Engineering and Technology (JEET)*, vol. 12, no. 1, 2017.

[10] A. S. Abdel-Khalik and S. M. Gadoue, "Improved flux pattern by third harmonic injection for multiphase induction machines using neural network," *Alexandria Engineering Journal*, vol. 50, no. 12, pp. 163-169, 2011.

[11] A. K. Mohamed, B. S. Marwa, B. F. Mouldi, and R. Habib, "Performance evaluation of self-excited DSIG as a stand-alone distributed energy resource," *Electrical Engineering, Springer*, vol. 97, no. 4, pp. 261-345, 2016.

[12] J. H. Alwash and L. J. Qaseer, "Three-dimension finite element analysis of a helical motion induction motor," *ACES Journal*, vol. 25, no. 8, pp. 703-712, Aug. 2010.

[13] A. Shiri and A. Shoulaie, "Investigation of frequency effects on the performance of single sided linear induction motor," *ACES Journal*, vol. 27, no. 6, pp. 497-504, June 2012.

[14] B. S. Marwa, A. K. Mohamed, B. F. Mouldi, and R. Habib, "Modeling and analysis of double stator induction machine supplied by multi-level inverter," *16th IEEE Mediterranean Electrotechnical Conference (MELECON), IEEE*, 2012.

[15] M. Hassani and A. Shoulaie, "Dynamic modeling of linear actuator using fuzzy system to approximate magnetic characteristics," *ACES Journal*, vol. 30, no. 8, Aug. 2015.

[16] A. K. Mohamed and R. Habib R, "General modeling of saturated AC machines for industrial drives," *COMPEL: The International Journal for Computation and Mathematics in Electrical and Electronic Engineering*, vol. 35, no. 1, pp. 44-63, 2016.